

Measurement of lens focal length using multi-curvature analysis of Shack-Hartmann wavefront data

Daniel R. Neal, James Copland, David A. Neal, Daniel M. Topa and Phillip Riera
WaveFront Sciences, Inc., 14810 Central S.E., Albuquerque, NM 87123

ABSTRACT

The lens is one of the most commonly used optical elements. Yet it is sometimes difficult to make accurate effective focal length and pupil position measurements, especially for long focal length lenses. Many measurement methods rely on a mechanical measurement to determine the back focal length, or may require careful operator discrimination in determining the best focus position. Aberrations may confuse an automatic focal length measurement system. However, an accurate determination of the optical properties of a lens is often critical for building an accurate system model.

We have developed a method for measurement of the focal length, pupil plane and collimation positions of positive lenses using a Shack-Hartmann wavefront sensor. The SHWFS uses a micro-optic lens array to separate the incoming wavefront into a pattern of focal spots. The position of these focal spots is related to the local wavefront slope. Wavefront reconstruction allows the complete incident wavefront to be retrieved. A Zernike decomposition reconstructor is used to separate the effects of lens focal power from other aberrations. The lens under test is illuminated by a point source on a computer-controlled stage. The transmitted wavefront was recorded by the SHWFS while the source was translated over a few mm range. By analyzing the Zernike coefficient associated with defocus, we were able to extract the focal length, pupil plane and collimation positions using a least squares fitting procedure.

This procedure was tested for a variety of lenses of varying focal lengths, from 10 to 1000 mm focal length, and showed excellent repeatability and accuracy. These measurements were compared to knife-edge, manufacturer's specification, and ray-tracing analysis for verification testing.

Keywords: Focal length, wavefront sensor, Shack-Hartmann, Hartmann-Shack, lens testing, optical testing, optical metrology, lens testing, focal length measurement, lens power, vergence

1 INTRODUCTION

The key property of the most common optical element, the lens, is its focal length. In almost every application it is important to know an accurate value for this property. Yet this is often a difficult parameter to accurately measure, especially for longer focal length (or lower numerical aperture) lenses. In addition, spherical and other aberrations may make measurement of the paraxial properties difficult and ambiguous. Thus a method for accurately determining this property would be useful for a number of applications.

Various methods have been used for measuring the focal lengths of lenses¹. During manufacture, it is common practice to use a test plate to determine the radius of curvature, and then, with a known index of refraction, the focal length may be calculated. The location of the principle plane requires some ray-tracing or other analysis, and the tolerances must be known in order to estimate the potential error. In many ways this may be the most accurate means for determining the focal length.

Other methods include knife-edge test, magnification test, auto-collimation, nodal slide bench, and minimum spot size. In most of these the measurement depends strongly on the aperture of the test, and a mechanical measurement must be made to some lens surface or edge. Thus the accuracy of the measurement may depend on knowledge of exactly how the lens is mounted.

For many applications, the most important parameter is the effective focal length². This is the distance from the principle plane to the focal point. This is the parameter that is used in thin lens equations and that is relevant for paraxial optical system design. Even for systems with aberrations, the effective focal length or paraxial performance is usually the baseline or starting condition.

One way to measure the focal length of a lens is to measure its image formation properties. This requires measurement of the object and image distances and then calculation using the thin lens equation. While this still requires mechanical measurements from some reference plane, and includes the effects of aberrations, it can produce good results for finding the effective focal length. Adopting a procedure that involves multiple measurements and utilizes a least squares error minimization approach can be used to reduce the effect of error of any individual measurement³.

With the advent of accurate wavefront sensors, it is possible to automate the acquisition and analysis process. The wavefront sensor also allows separation of the paraxial (focus) parameters from other higher order effects (such as spherical aberration or coma). This paper describes an extension of the method presented by Pernick and Hyman³ using a Shack-Hartmann wavefront sensor.

2 SHACK HARTMANN WAVEFRONT SENSING

Shack Hartmann wavefront sensing has matured significantly in the last several years. While historically these sensors were used for adaptive optics in astronomy and high energy lasers, they have recently been applied to a wide range of problems, including laser beam characterization^{4,5}, fluid turbulence measurement^{6,7,8}, optical system alignment⁹, ophthalmic metrology¹⁰, wafer metrology¹¹, optical metrology for both large¹² and small¹³ optics.

2.1 Principle

The basic measurement principle is similar to the Hartmann test of the early 1900s. In this test, a mask with holes was placed in front of the lens to be tested. Light passing through the holes was examined at two planes, typically before and after the focal plane. This allowed a kind of physical ray tracing of the optic. By examining the shift in position of the rays compared to that of an ideal lens, the aberrations, wavefront map, MTF, and other parameters could be determined.

In the late 1960s, Roland Shack proposed first shifting the measurement plane to the pupil plane and then using a grid of lenslets to sample larger areas¹⁴, while still providing measurements over sub-apertures.

Figure 1 shows the arrangement of a typical modern Shack-Hartmann sensor. In this case a lenslet array, fabricated using photolithography and etching in fused silica, is used to collect the light and direct it onto a CCD array sensor. The grid of pixels on the CCD array provides an accurate measurement of the focal spot positions.

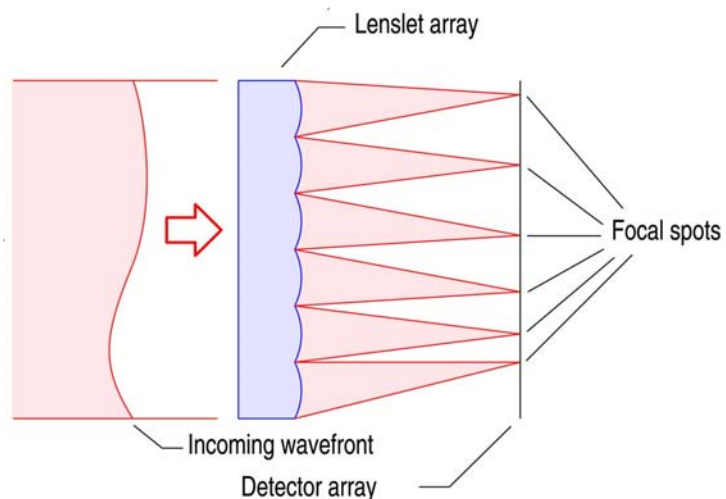


Figure 1 Basic arrangement of a Shack-Hartmann wavefront sensor.

The lenslet array breaks up the incident wavefront into a large number of small sub-apertures. The key assumption is that, over each sub-aperture, the only wavefront variation is local tilt. This is readily achieved with sufficiently high-resolution lenslet¹⁵. The light from each of these samples is collected by the lenslet and focused on the detector. Since the region is small, this usually creates a well-formed focal spot whose position is shifted corresponding to the

local wavefront tilt. The CCD detector records this focal spot position, and so, by comparison against a reference, the local slope can be determined. With a large number of local slope measurements, the wavefront surface can be numerically reconstructed.

Since the information for all of the focal spots is obtained simultaneously, all of the needed information is obtained in a single CCD frame. With modern CCD camera systems very short exposure times can be used. If there is tilt caused by vibration that occurs between successive frames, it will result in a lateral shift of all the focal spots on the CCD. This is readily identified and subtracted out (or measured if it is useful). The single frame acquisition also means that if the wavefront structures are dynamic (that is, changing rapidly), the instantaneous wavefront will be measured with little error.

The focal spot locations are usually determined by an algorithm called the centroid algorithm^{*}:

$$\bar{x}_k = \frac{\sum_{j \in AOI_k} x_j S_j}{\sum_{j \in AOI_k} S_j}, \quad (1)$$

where S_j is the modified irradiance distribution over a region AOI_k corresponding to the light from a particular lenslet. A similar equation applies for the y-coordinate of the spot locations. Typically, a threshold algorithm is applied to the irradiance distribution to produce the modified distribution, although other algorithms may apply (deconvolution, for instance).

A reference beam is recorded for use in determining the wavefront gradients from the spot position measurements. Usually this is obtained by recording a plane wave, although the reference may also be calculated numerically. This provides a set of reference centroids x_k^{ref} and y_k^{ref} .

The wavefront gradient for each location k on the sensor is:

$$\begin{pmatrix} \beta_x \\ \beta_y \end{pmatrix}_k = \frac{1}{f} \begin{pmatrix} \bar{x} - x_{REF} \\ \bar{y} - y_{REF} \end{pmatrix}_k \quad (2)$$

where f is the lenslet to detector spacing, which is usually set to the focal length of the lenslet.

The wavefront gradients are connected by the assumption that the wavefront is continuous. While there are some situations where this assumption breaks down, for these very small lenslets it is usually quite realistic. Thus for each point k on the sensor lenslet coordinates (x_k, y_k) :

$$\nabla w = \frac{\partial w}{\partial x} \vec{i} + \frac{\partial w}{\partial y} \vec{j} = \beta_k^x \vec{i} + \beta_k^y \vec{j} \quad (3)$$

which is just the definition of the gradient in terms of the scalar field $w(x,y)$, except that we have substituted the measured local gradients β_x and β_y .

This equation can be solved for the wavefront $w(x,y)$ in a number of ways. The surface can be described in terms of polynomials, and then a least squares fit routine can be used to find the appropriate coefficients. This is the so-called Modal method. Alternatively, the slope data can be used to solve for a self-consistent set of wavefront heights.

2.2 Wavefront curvature

The wavefront curvature can be derived directly from the solution to Equation 3 through the use of a polynomial expansion:

^{*} This is actually a misnomer. It would more accurately be called a center-of-mass algorithm, since it includes a weighted distribution in the calculation, and not just the shape of the boundary. For connection with the literature in this subject, we've continued to use the term centroid to refer to the determination of these spot positions.

$$w(x, y) = \sum_k C_k P_k(x, y) \quad (4)$$

where the polynomials $P_k(x, y)$ can be any from the Taylor, Zernike, Tchevechev or other polynomials. These polynomials need not necessarily be orthogonal, but there are certain advantages if orthogonal polynomials are used. Following the methods of Southwell¹⁶, the analytical expression for the wavefront slope at each point (x, y) is given as:

$$\begin{pmatrix} \frac{\partial w}{\partial x} \\ \frac{\partial w}{\partial y} \end{pmatrix} = \begin{pmatrix} \sum_k C_k \frac{\partial P_k}{\partial x} \\ \sum_k C_k \frac{\partial P_k}{\partial y} \end{pmatrix} \quad (5)$$

A merit function that describes the fit error of the in terms of the polynomial expansion coefficients may be formed using all the data acquired at each point (x_i, y_i) :

$$\chi^2 = \sum_i \left[\left(\beta_x(x_i, y_i) - \sum_k C_k \frac{\partial P_k(x_i, y_i)}{\partial x} \right)^2 + \left(\beta_y(x_i, y_i) - \sum_k C_k \frac{\partial P_k(x_i, y_i)}{\partial y} \right)^2 \right] \quad (6)$$

This may be minimized with respect to the fit coefficients C_k to find the solution for the wavefront surface. The wavefront curvature is that portion of the wavefront that may be described by a sphere. That is:

$$w_c(x, y) = \sqrt{R^2 - (x^2 + y^2)} \quad (7)$$

for a paraxial system this may be written:

$$w_c(x, y) \approx \frac{x^2 + y^2}{2R} \quad (8)$$

It should be noted that the focal length of a lens is a paraxial property. Expansion of the wavefront in terms of Zernike polynomials provides a convenient means for expressing the wavefront in terms of various optical aberrations. The wavefront curvature, spherical aberration, coma, trefoil and other aberrations may be expressed directly in terms of specific polynomials¹⁷. One advantage of the use of Zernike decomposition is that the paraxial curvature may be separated from other, higher order, effects.

3 MULTI-CURVATURE ANALYSIS

The Shack-Hartmann wavefront sensor (SHWFS) is capable of measuring the radius of curvature of the incident wavefront with excellent accuracy. This can be used in the analysis of optical system parameters. This is particularly relevant for analysis of the focal length of lenses, or for calibration of the wavefront sensor itself. Pernick and Hyman describe a method for measuring the focal lengths of lenses by finding conjugate image/object locations³. A least squares fit was used with some accuracy to find the lens parameters. In this early work, the image plane location was determined simply by looking for the location of best focus. However, this requires some judgment on the part of an operator, and for lenses with significant aberrations it would be difficult to separate the effects of the paraxial property focal length from other effects such as spherical aberration.

3.1 Analysis

Figure 2 shows the basic geometry for measuring optical system parameters using a wavefront sensor to measure the radius of curvature as the source (S) position (Z) is varied. In this figure, Z_0 is the location of the source for a collimated beam, Z is the stage position of the source at a measurement point, f is the focal length of the lens, L is the distance from the wavefront sensor to the principle plane of the lens, and R is the measured radius of curvature on the wavefront sensor.

The radius of curvature R may be calculated from the wavefront sensor measurement as:

$$R = -\frac{a^2}{4C_{21}}, \quad (9)$$

where a is the radius of the circle used to calculate the Zernike coefficient, and C_{21} is the coefficient for the defocus term. This polynomial is given by:

$$Z_{21}(x, y) = 2\left(\frac{x}{a}\right)^2 + 2\left(\frac{y}{a}\right)^2 - 1 \quad (10)$$

where x and y are the coordinates across the aperture.

The lens obeys the thin lens formulation, that is:

$$\frac{1}{f} = \frac{1}{s_o} + \frac{1}{s_i}. \quad (11)$$

Replacing this with the relevant parameters results in:

$$\frac{1}{f} = \frac{1}{f + Z - Z_0} + \frac{1}{R + L}. \quad (12)$$

Note that the radius of curvature will go to infinity at collimation (this is the definition of collimation). To avoid including parameters that go through infinity in the analysis, we formulate instead the mathematics in terms of the measured vergence (or power) at the wavefront sensor. That is:

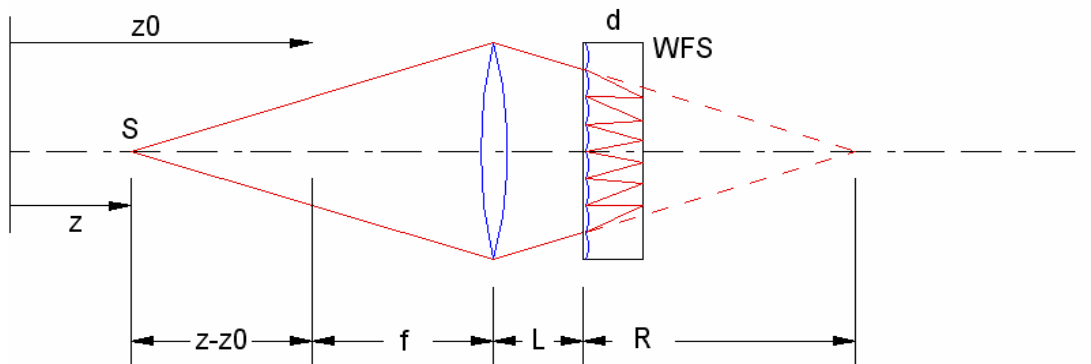


Figure 2 Multi-curvature analysis of a lens element

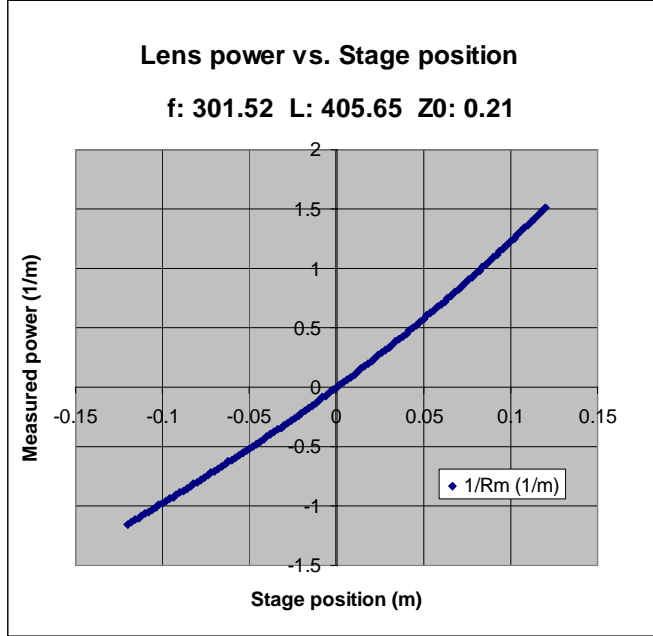


Figure 3 – Measured lens power ($1/R$) as a function of stage position for a 301 mm focal length lens.

the calibration of the wavefront sensor is known, then a fit of Equation 14 with parameters f , L , and Z_0 can accurately be used to predict this curve.

Figure 4 shows the measured lens power compared to the predicted power from equation 14. The residual error is also shown in this figure (plotted against a different scale shown on the right). One method for calibrating the wavefront sensor (determining the distance between lenslet array and detector) is to calculate the slope of this line. Any deviation from 1 will be the result of an incorrect distance used in the analysis of the slope data, which linearly propagates through the analysis.

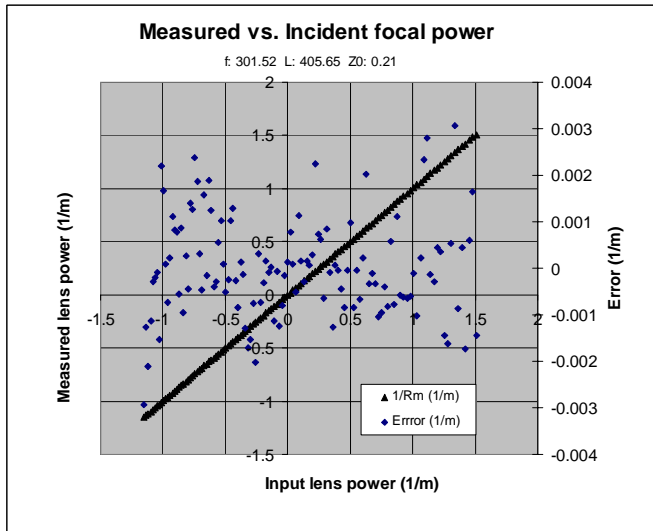


Figure 4 Measured lens power ($1/R$) as a function of calculated incident power.

$$P = \frac{1}{R}. \quad (13)$$

Solving Equation 12 for the power $1/R$ yields:

$$P(z) = \frac{1}{R} = \frac{z - z_0}{f^2 + (f - L)(z - z_0)} \quad (14)$$

This allows us to plot the measured power as a function of the expected power, given a sequence of measurements, if the various lens parameters are known. It is also possible to determine the lens parameters (f , L , Z_0) from a sequence of measurements using a least squares fit procedure.

3.2 Measurement

Figure 3 shows an example of a measurement for a 301 mm focal length lens. In this case 101 measurements were acquired with the position of the source varied over a +/-12 mm range. If the

4 SOLUTION METHODS

The key solution task is to solve for the parameters f , L , and z_0 . This can be done through a least squares fit procedure. An expression for the square error can be written:

$$\chi^2 = \sum_i [P_i - P(z_i)]^2 \quad (15)$$

where P_i is the measured power at each point z_i , and $P(z_i)$ is Eq. 14 evaluated at z_i . Equation 14 is non-linear in the parameters of interest. This makes retrieving the focal length and other parameters more difficult. Several different methods will be examined in the following sections.

4.1 Quadratic fit

Examination of Figure 3 indicates that, over a typical range of interest, the non-linearity is often fairly

weak. By changing variables, Equation 14 can be rewritten as:

$$P = \frac{\zeta}{A + B\zeta} \quad (16)$$

where $\zeta = z - z_0$, $A = f^2$, and $B = f - L$. For the case where $A \gg B\zeta$, the binomial expansion can be used to obtain an approximate expression. Thus Equation 16 becomes:

$$P \approx \frac{\zeta}{A} \left[1 - \frac{B}{A} \zeta \right]. \quad (17)$$

Recalling that $\zeta = z - z_0$, we recognize that this equation is a quadratic:

$$P = Dz^2 + Ez + F \quad (18)$$

where $D = -B/A^2$, $E = (1 + 2z_0B/A)/A$, and $F = -(z_0/A)(1 + Bz_0/A)$. Equation 18 may now be fit with a linear least squares fit routine and the parameters D , E and F readily obtained. Once these parameters are known, f , L , and z_0 may be uniquely determined.

4.2 Newton lens formulation - iterative fit

The wavefront sensor offers a convenient measurement of focal length by using the Newtonian form of the lens

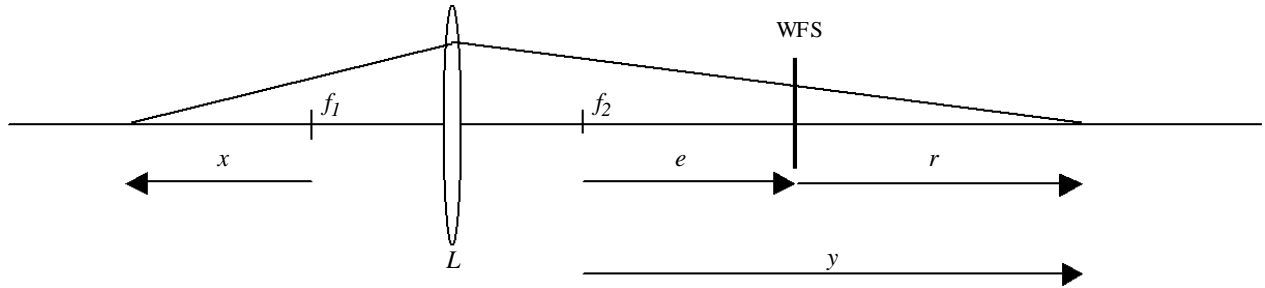


Figure 5 Schematic of the experimental setup. The lens of interest is denoted by L. A wavefront sensor WFS is placed an unknown distance downstream from the lens. A point source is then placed at the collimation point f1, the collimation being verified with a shear plate. Then, a precision stage is used to move the point source a distance x from collimation. As the source moves away from collimation, the wavefront sensor will record smaller radii of curvature. The radius or curvature r is the sum showing the sign convention. As drawn, $x < 0$, and the parameters e, r, and y are all greater than zero.

equation as shown in Hecht¹⁸, p. 163. The figure below defines the observed and free parameters.

The measured quantities are x , the varied distance between the source and the lens and r , the measured curvature. The computed parameters are e , the distance between the lenslet array and, f_2 and f_1 , the focal length of the lens L . The Newtonian form of the lens equations cited is (with a reversed sign convention)

$$xy = -f^2 \quad (19)$$

which can be reposed in terms of the measured and computed parameters as

$$x(r + e) = -f^2. \quad (20)$$

This functional relationship defines the fit. If we make the substitution $\phi = f^2$ we have a linear problem which can be directly solved using the method of least squares.

Consider a measurement series comprised of N data points of the form (x_i, r_i) . We can define the best fit as the parameters ϕ and e , which minimize the merit function

$$\chi^2 = \sum_{i=1}^N \frac{[x_i(r_i + e) + \varphi]^2}{\sigma_i^2}. \quad (21)$$

where the errors σ_i are for now considered to be equal, relegating them to a superfluous multiplicative constant. These terms will be reintroduced at the end. Also, to reduce visual clutter we will abandon the explicit bounds on the summation terms since all summations are over all N data points.

As always we find extrema by solving the equations when the first derivatives are set equal to zero. In other words we simultaneously require that

$$\frac{\partial \chi^2}{\partial \varphi} = 0 \text{ and } \frac{\partial \chi^2}{\partial e} = 0. \quad (22)$$

The resulting two linear equations can be solved immediately

$$\begin{pmatrix} e \\ \varphi \end{pmatrix} = -\frac{1}{\Delta} \begin{pmatrix} N \sum x_i^2 r_i - \sum x_i r_i \sum x_i \\ \sum x_i r_i \sum x_i^2 - \sum x_i^2 r_i \sum x_i \end{pmatrix}. \quad (23)$$

where the determinant is given by

$$\Delta = N \sum x_i^2 - \left(\sum x_i \right)^2. \quad (24)$$

The error propagation has one small wrinkle in it; otherwise we follow the standard methodology. See, for example, Bevington¹⁹, chap. 6. The error terms are

$$\begin{pmatrix} \sigma_e^2 \\ \sigma_\varphi^2 \end{pmatrix} = \frac{s^2}{\Delta^2} \begin{pmatrix} \left(\sum x_i \right)^2 \sum x_i^2 + N^2 \sum x_i^4 - 2N \sum x_i \sum x_i^2 \\ \left(\sum x_i^2 \right)^2 \left(\sum x_i^2 + \sum x_i^4 \right) - 2N \sum x_i \sum x_i^2 \sum x_i^3 \end{pmatrix}. \quad (25)$$

where the parent sample variance (Bevington¹⁹, p. 114) is approximated by the experimental variance

$$s^2 = \frac{1}{N-3} \sum (x_i(r_i + e) + \varphi)^2. \quad (26)$$

The wrinkle is that we are interested in the error propagation for the focal length f , not the parameter φ . We simply need to invert the formula for the error in a quadratic term (see for example Bevington¹⁹, p. 61). The error in a quadratic measurement g is simply

$$(g \pm \sigma_g)^2 \rightarrow g^2 + \sqrt{2g^2 \sigma_g^2}. \quad (27)$$

We are now able to relate the computed error in the parameter φ to the error in the focal length:

$$\sigma_f^2 = \frac{1}{2} \frac{\sigma_\varphi^2}{\varphi}. \quad (28)$$

This method works quite well when the collimation of the system is well known. However, practical laboratory measurements may not allow for precise determination of the collimation point. In these cases, we generalize the development to include an offset term δ .

The new merit function becomes

$$\chi^2 = \sum_{i=1}^N \frac{[(x_i + \delta)(r_i + e) + \varphi]^2}{\sigma_i^2}. \quad (29)$$

Lamentably, the fitting parameters e , φ , and δ are no longer linear. As an example, consider first derivative (ignoring the σ 's) for the e parameter:

$$\sum ((x_i + \delta)(r_i + e) + \varphi)(x_i + \delta) = \sum (\delta^2(e + r_i) + \delta(2ex_i + 2x_i r_i + \varphi) + x_i^2(e + r_i) + x_i \varphi) = 0. \quad (30)$$

Clearly there is no hope of posing a linear system like

$$\begin{pmatrix} f_1(x) & f_2(x) & f_3(x) \\ f_2(x) & f_4(x) & f_5(x) \\ f_3(x) & f_5(x) & f_6(x) \end{pmatrix} \begin{pmatrix} e \\ \varphi \\ \delta \end{pmatrix} = \begin{pmatrix} g_1(x, y) \\ g_2(x, y) \\ g_3(x, y) \end{pmatrix} \quad (31)$$

and we are driven to an of a number of iterative methods.

4.3 Full non-linear iterative fit

The parameters f , L and z_0 can be determined through a least squares fit procedure. The expression for the sum-squared error, Eq. 15, is differentiated with respect to the various parameters (f , L , and z_0), is set equal to zero to find the location of minimum error:

$$\frac{\partial \chi^2}{\partial f} = -2 \sum (P_i - P(z_i)) \frac{\partial P}{\partial f} = 0, \quad (32)$$

and similarly for L and z_0 . This results in three independent non-linear equations in f , L , and z_0 that must be solved simultaneously to arrive at the solution for the parameter values. While there are a number of standard methods for obtaining such solutions, they usually involve some form of iterative solution methodology. It should be noted that the quadratic fit method will generally give a very good starting value for all the parameters. This allows the iterative fit routine to only slightly adjust the parameter values, thereby minimizing any problems with instability or erroneous solutions.

5 ERROR ANALYSIS

Equation 14 can be evaluated to determine the sensitivity of the measured parameters to the noise or error in the experimental data. While Equation 15 yields a value for the residual RMS fit error, this does not give a representation of the error in determining the parameters f , L and z_0 . The error in these parameters can be written:

$$\delta f = \frac{\partial f}{\partial P} \delta P \quad (33)$$

$$\delta L = \frac{\partial L}{\partial P} \delta P \quad (34)$$

$$\delta z_0 = \frac{\partial z_0}{\partial P} \delta P. \quad (35)$$

Although a better formulation may be to use the method of Bevington, Chapter 4¹⁹. Equation 14 can then be evaluated to produce the required derivatives:

$$\frac{\partial f}{\partial P} = -\frac{z - z_0}{2fP^2} \quad (36)$$

$$\frac{\partial L}{\partial P} = \frac{1}{P^2} + \frac{z - z_0}{2fP^2} \quad (37)$$

$$\frac{\partial z_0}{\partial P} = -\frac{z - z_0}{P(1 + (f + L)P)} \quad (38)$$

The expected error in each of the parameters can thus be evaluated by using Eq. 33-35, given the derivative expressions 36-38, to form an error estimate for each point. The root mean square error evaluated at all the measurement points gives a measure of the expected error.

6 RESULTS

This method for measuring the focal length of a lens was used to measure the focal lengths of three lenses with widely differing characteristics. These lenses had focal lengths of ~300 mm, 50 mm, and 37 mm. The 300-mm and 50-mm lenses were both doublets, while the 37-mm was an extremely fast ($f\#$ 0.74) multi-element lens. These lenses were measured in place in a contact lens mold metrology instrument that had built-in alignment and adjustment stages for moving various parts of the apparatus. By placing a bare fiber end on the appropriate stage, the data could readily be recorded as needed by the multi-curvature analysis (MCA) method.

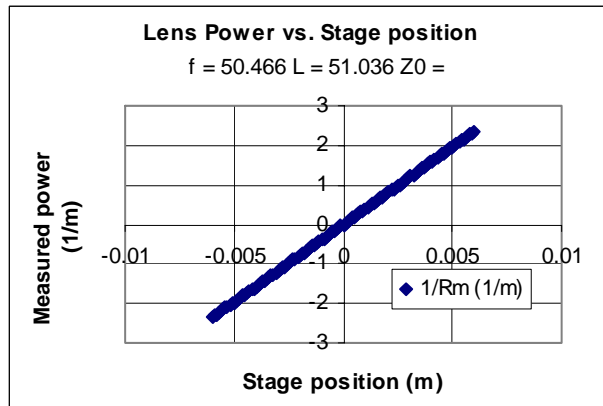


Figure 7– Measured lens power ($1/R$) as a function of stage position for a 50 mm focal length lens.

6.1 Comparison of analysis methods

For the three lenses described in Figure 3, Figure 7 and Figure 6, we calculated the lens parameters (f , L and z_0) using the three methods described in section 4. Solutions were obtained using both a programmed Visual Basic implementation and using the numerical solver in Microsoft Excel. Variations are expected only through differences in precision of the two programs. The comparison of the residual fit error (Eq. 15) is shown in Figure 8 where, except for Lens L3 (37 mm f.l.), the values are very low. For this lens the measurement plane is considerably different from $f = L$.

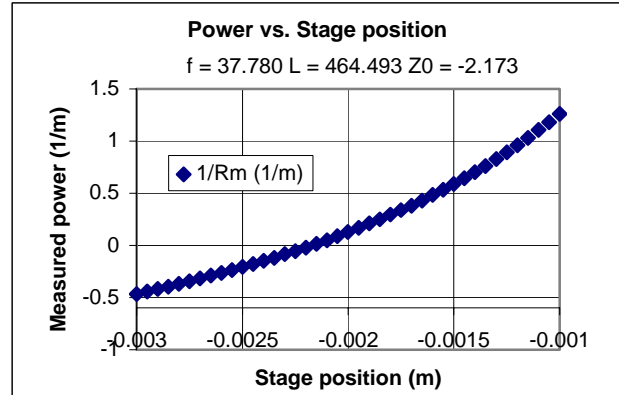


Figure 6– Measured lens power ($1/R$) as a function of stage position for a 37 mm focal length lens.

Figure 7 shows the measure power as a function of stage position for a ~50 mm lens, where the distance from the lenslet array to the lens is about equal to the focal length of the lens. Notice in Eq. 14 that, for $f = L$, the equation becomes entirely linear with slope $1/f^2$. This is also evident in Figure 7.

In Figure 6 a ~37 mm focal length lens was measured where the lens was placed a considerable distance from the wavefront sensor. In this case the curve is not linear, indicating that $f - L$ is not near zero.

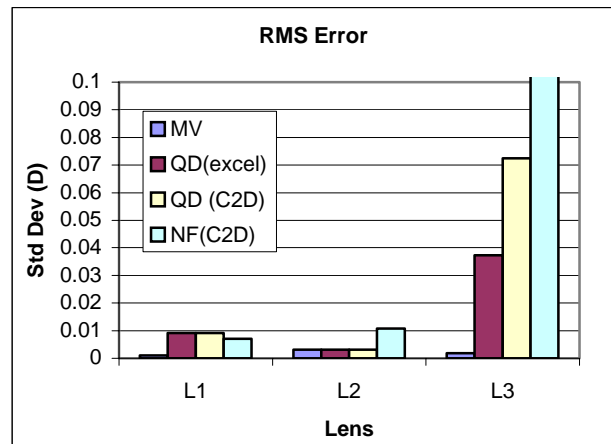


Figure 8– Residual RMS error (power) for the three lenses using the different analysis methods. MV is the fully non-linear fit method, QD is the Quadratic fit method, and NF is the Newton fit method.

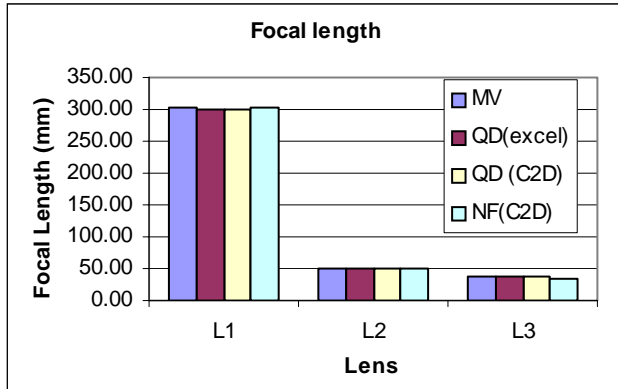


Figure 9– Lens focal length for the three lenses using the different analysis methods.

should be reasonable accuracy in determining this position. However, the wavefront sensor can accurately make measurements of radii that are many tens of meters. For a distance L that is a few tens of mm, the accuracy may not be sufficient due to numerical instabilities. This can also be seen in Eq. 37, where the error grows as $1/P^2$. For nearly collimated measurement points, P is near zero, and so the error in Equation 37 grows rather large.

Figure 10 shows the lens to detector distance calculated with the different methods. While the methods agree fairly well for the cases where the lens is near the detector, the calculated distance has considerable variation for the case with a larger measurement plane distance. For all these cases the actual distance agrees closely with the non-linear fit method (MV).

This introduces more non-linearity, which makes the analysis more sensitive to approximations and assumptions. Note that the fit error is still very low for the full iterative fit (MV) case.

The variation in the measured focal length is shown in Figure 9. In all cases the focal length is very close to the same number, even for the lens that was distant from the WFS (L3). The actual variation in the various positions is less than 0.3% in all cases.

The distance between the wavefront sensor lenslet array and the principle plane of the lens is somewhat harder to measure with this method. This is easiest to see by noting that this distance enters through Eq. 12 by addition with the radius of curvature measured by the wavefront sensor. As long as the radii and this measurement plane distance are comparable, there

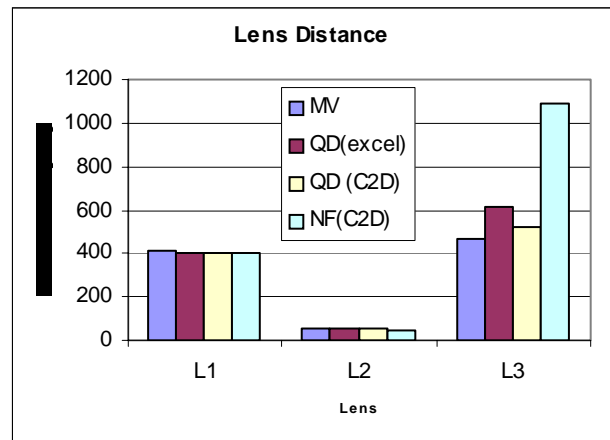


Figure 10– Lens to measurement plane distance for the three lenses using the different analysis methods.

7 ACCURACY AND REPEATABILITY

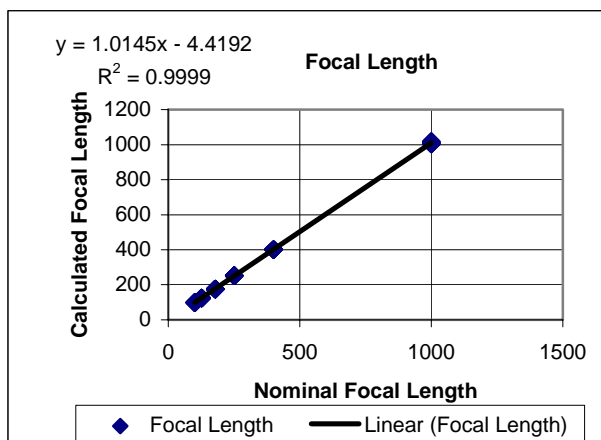


Figure 11 – Lens focal length for various lenses measured using the multi-curvature method. For each focal length, ten separate measurements are plotted.

To assess the repeatability of the focal length measurement process, we conducted an R&R reproducibility study. To this end, a number of lenses were repeatedly measured. Figure 11 shows the measured focal lengths for six different lenses from 100 mm to 1000 m focal lengths. While it appears that only one point is plotted for each focal length, in each case ten different measurements are plotted on the graph, but the points lie on top of each other. The data correlates with the nominal focal length (obtained from the manufacturer) almost perfectly, $R^2=0.9999$. The slope of 1.0145 shows a 1.4% error in measured focal length. This, in fact, may be biased by the measurements at the longer focal lengths where the nominal focal length may not be known as well. In this case there is considerable error in the nominal focal length (which is unknown).

The measurement of the principle plane distance to the lenslet array is not so certain. Figure 12 shows the determination of the measurement plane distance for a 500 mm focal length lens where the wavefront sensor was set at different distances. Note that there is considerable scatter in the data for each measurement location while the general trend is apparent. The correlation between measured data and the WFS position is only 0.89 with an R^2 of 0.86. This can be understood if the range of measured powers is also considered. The point source was moved by only ± 40 mm for this lens, resulting in (according to Eq. 14) a total maximum diopter power of 0.15 D. This represents a maximum wavefront radius of curvature of over 6 m. Hence it is not surprising that it is difficult to determine a parameter with much smaller value that is added to the measured radius of curvature (according to E. 12). To obtain an accurate measure for this parameter, the values of the measured radius of curvature and the measurement plane distance would have to be comparable.

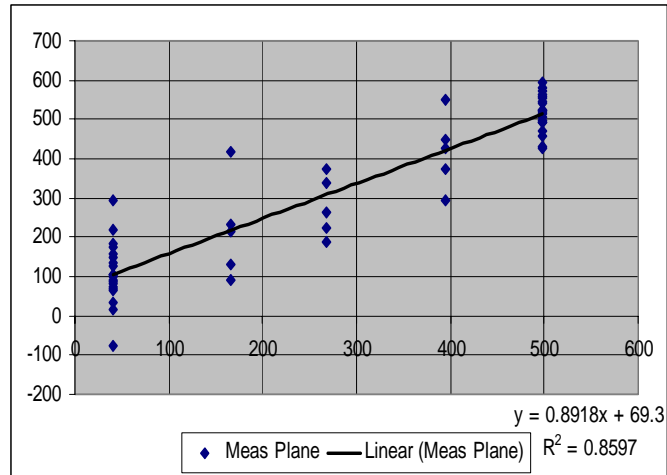


Figure 12 – MCA method determined measurement plane distance (distance from lenslet array to lens principle plane) for a 500 mm lens as a function of lens distance.

It should be understood that, similar to the measurement of the principle plane of Pernick and Hyman³, the principle plane of the lens is still accurately determined. That is because it is not the measurement plane distance, L , that is the correct value to use for determining the principle plane, but the collimation position Z_0 . If the lens and stage are arranged so that there is a fixed mechanical relationship between some surface of the lens and some position of the stage, then Z_0 can be used to determine the exact location of the measurement position.

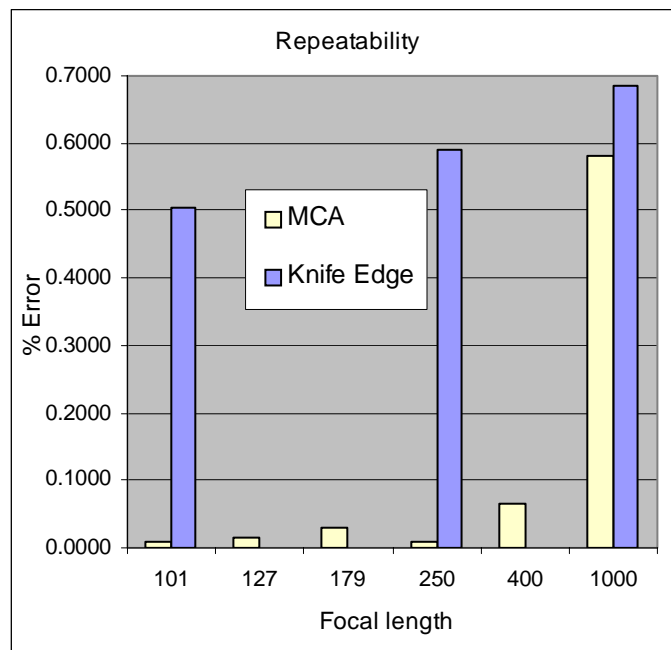


Figure 13– Repeatability of ten measurements using the MCA method for several different focal lengths. The repeatability of measuring the focal length of the same lenses using the knife-edge method is also shown for comparison.

In Figure 13, the repeatability of measuring the focal length is shown more explicitly than in Figure 11. In this case the standard deviation is shown for all the measurements for six different lenses. Also shown is the measured repeatability for ten measurements using the Foucault knife-edge technique. Surprisingly, this technique had about the same percent error for all the focal lengths. By comparison, the MCA method had significantly improved repeatability for the shorter focal lengths, and better repeatability in all cases.

8 CONCLUSION

We have developed a method for measuring the focal length of lenses with excellent accuracy. Several different methods for determining the focal length, measurement plane distance and collimation position were developed and tested. It was routinely possible to make measurements that were better than 0.5% in the focal length (usually less than 0.1%); however, instability in the formulation causes difficulty in determining the measurement plane accurately. The focal length calculation compared to the knife-edge method showed

improved repeatability in most cases.

9 ACKNOWLEDGEMENTS

The authors would like to acknowledge Isaac Neal for help with data acquisition and analysis.

10 REFERENCES

- 1 Jurgen R. Meyer-Ardent *Introduction to Classical and Modern Optics*, Prentice Hall, 1972
- 2 R. R. Rammage, D. R. Neal, R. J. Copland, "Application of Shack-Hartmann wavefront sensing technology to transmissive optic metrology," *SPIE* **4779-27** (2002).
- 3 J. B. Pernick and B Hyman, "Least-squares technique for determining principal plane location and focal length," *Appl. Optics* **26**(15), pp. 2938-2939 (1987).
- 4 D. R. Neal, W. J. Alford, and J. K. Gruetzner, "Amplitude and phase beam characterization using a two-dimensional wavefront sensor", *SPIE* **2870**, pp.72-82 (1996).
- 5 D. R. Neal, J. K. Gruetzner, D. M. Topa, J. Roller, "Use of beam parameters in optical component testing," *SPIE* **4451**, pp. 394-405 (2001).
- 6 W. J. Yanta, W. C. Spring, III, J. F. Lafferty, A. S. Collier, R. L. Bell, D. Neal, D. Hamrick, J. Copland, L. Pezzaniti, M. Banish, R. Shaw, "Near-and far-field measurements of aero-optical effects due to propagation through hypersonic flows," *AIAA-2000-2357* (2000).
- 7 Neal, D.R., Hedlund, E., Lederer, M., Collier, A., Spring, C., Yanta, W., "Shack-Hartmann Wavefront Sensor Testing of Aero-optic Phenomenon," *AIAA 98-2701, 20th AIAA Advanced Measurement and Ground Testing Technology Conference*, Albuquerque, NM, June 1998.
- 8 Neal, D.R., O'Hern., Torczynski, J.R., Warren, M.E. and Shul, R., "Wavefront Sensors for Optical Diagnostics in Fluid Mechanics: Applications to Heated Flows, Turbulence and Droplet Evaporation," from *Optical Diagnostics in Fluid and Thermal Flows, SPIE 2005*, 1993.
- 9 D. R. Neal and J. Mansell, "Application of Shack-Hartmann Wavefront Sensors to Optical System Calibration and Alignment," *Proceedings of the 2nd International Workshop on Adaptive Optics for Industry and Medicine*, Gordon Love, Ed., World Scientific (2000).
- 10 D. R. Neal, D. M. Topa, and James Copland "The effect of lenslet resolution on the accuracy of ocular wavefront measurements," *SPIE* **4245** (2001).
- 11 T.D. Raymond, D.R. Neal, D.M. Topa, and T.L. Schmitz, "High-speed, non-interferometric nanotopographic characterization of Si wafer surfaces," *SPIE* **4809-34**, 2002.
- 12 D. R. Neal, P. Pulaski, T.D. Raymond, and D. A. Neal, "Testing highly aberrated large optics with a Shack-Hartmann wavefront sensor," *SPIE* **5162**, 2003.
- 13 D. R. Neal, D. J. Armstrong and W. T. Turner, "Wavefront sensors for control and process monitoring in optics manufacture," *SPIE* **2993**, pp. 211-220, 1997.
- 14 B. Platt, R. Shack, "History and principles of Shack-Hartmann wavefront sensing" *Journal of Refractive Surgery*, **17** (Sept/Oct 2001).
- 15 D. R. Neal, J. Copland, D.A. Neal, "Shack-Hartmann wavefront sensor precision and accuracy," *SPIE* **4779**, 2002.
- 16 W.H. Southwell "Wave-front estimation from wavefront slope measurements" *JOSA* **70**, pp.993-1006 (August 1980)
- 17 D. Malacara, *Optical Shop Testing 2nd Ed.*, John Wiley & Sons, New York
- 18 E. Hecht, *Optics*, 3rd edition, Addison-Wesley (1998).
- 19 P. R. Bevington, *Data Reduction and Error Analysis for the Physical Sciences*, McGraw-Hill, N.Y. (1969).